 CMES, vol.2, no.2, pp.273-289, 2001

Determination of Crack Tip Fields in Linear Elastostatics by the Meshless Local Petrov-Galerkin (MLPG) Method

H.-K. Ching and R. C. Batra[1]

Abstract: It is shown that the MLPG method augmented with the enriched basis functions and either the visibility criterion or the diffraction criterion successfully predicts the singular stress fields near a crack tip. Results are presented for a single edge-cracked plate and a double edge-cracked plate with plate edges parallel to the crack axis loaded in tension, the single edge-cracked plate with one plate edge parallel to the crack axis clamped and the other loaded by tangential tractions, and for a double edge-notched plate with the side between the notches loaded in compression. For the first three problems, the stress intensity factors computed with the equivalent domain and the contour integrals are found to agree well with those available in the literature. For the edge-notched plate, results computed with the MLPG method agree well with those obtained from the finite element method.

keyword: Singular fields, stress intensity factors, mixed-mode deformations, edge-cracked plates, edge-notched plates.

1 Introduction

Atluri and Zhu (1998, 2000), Kim and Atluri (2000), Atluri et al. (1999a,b) and Lin and Atluri (2000) have recently developed the meshless local Petrov-Galerkin (MLPG) approach and have applied it to analyze several linear elastostatics and convection-diffusion problems. We refer the reader to their papers for a review of the developments in meshless methods and how the MLPG technique differs from the other so-called meshless methods. More specifically, Atluri et al. (1999a) discuss the generality of the MLPG method in choosing the local basis for the trial and the test functions of a wide variety, leading to either symmetric or asymmetric system of equations.

Recently, Kim and Atluri (2000) demonstrated the use of the MLPG formulation, in conjunction with the use of secondary nodes and no special crack tip modeling, for finding elastostatic deformation fields near the crack tip. Here, on the other hand, we use the MLPG method in conjunction with either the visibility criterion of Belytschko et al. (1994) or the diffraction criterion of Organ et al. (1996) to analyze deformation fields near a crack tip. It is found that singular fields near a crack tip in a single edge-cracked plate and a double edge-cracked plate with the sides parallel to the crack subjected to uniformly distributed tensile surface tractions, in a single edge-cracked plate with one side parallel to the crack clamped and the other loaded by tangential surface tractions, and a double edge-prenotched plate with the edge between the two notches loaded in compression can be successfully computed with the present MLPG method which is augmented with the known crack-tip singular fields.

2 Formulation of the Problem

2.1 Governing equations

In rectangular Cartesian coordinates, the static deformations of an isotropic homogeneous linear elastic body are governed by the following equations:

$$\sigma_{ij,j} + b_i = 0, \text{ in } \Omega, \ (i,j = 1,2,3), \tag{1}$$

$$\sigma_{ij} = \lambda \varepsilon_{kk} \delta_{ij} + 2\mu \varepsilon_{ij}, \text{ in } \Omega, \tag{2}$$

$$\varepsilon_{ij} = (u_{i,j} + u_{j,i})/2, \text{ in } \Omega, \tag{3}$$

$$u_i = \overline{u}_i, \text{ on } \Gamma_u, \tag{4a}$$

$$t_i \equiv \sigma_{ij} n_j = \overline{t}_i, \text{ on } \Gamma_t. \tag{4b}$$

Here σ is the stress tensor, ε the infinitesimal strain tensor, $\mathbf{u}$ the displacement, $\mathbf{b}$ the density of body forces, a comma followed by the index i denotes partial differentiation with respect to x_i, a repeated index implies summation over the range of the index, $\mathbf{x}$ is the present position

[1] Department of Engineering Science and Mechanics, MC 0219
Virginia Polytechnic Institute and State University
Blacksburg, VA 24061, USA

of a material point, Ω the region of space occupied by the body, Γ_u and Γ_t are disjoint parts of the boundary $\partial\Omega$ of Ω, i.e., $\Gamma_u \cap \Gamma_t = \phi$, $\Gamma_u \cup \Gamma_t = \partial\Omega$, $\overline{\mathbf{u}}$ the prescribed displacements on Γ_u, $\overline{\mathbf{t}}$ the prescribed surface tractions on Γ_t, $\mathbf{n}$ an outward unit normal to Γ, and λ and μ are Lamé constants for the material of the body. Substitution from (2) and (3) into (1) yields second order partial differential equations for $\mathbf{u}$ which are to be solved under the boundary conditions (4).

2.2 Weak formulation

The following brief derivation of the local symmetric weak form (LSWF) follows that given by Atluri and Zhu (1998, 2000) and Lin and Atluri (2000) and is included for the sake of completeness. Even though the derivation is valid for a three dimensional problem, we restrict ourselves to two-dimensional problems. Thus, the range of indices i and j is 1,2.

Let $\Omega_s \subset \Omega$ be a subdomain of Ω, $\Gamma_s = \partial\Omega_s \cap \partial\Omega$, $L_s = \partial\Omega_s - \Gamma_s$ and $\mathbf{v}$ be a smooth function defined on Ω_s that vanishes on L_s. Let $\Gamma_{su} = \Gamma_s \cap \Gamma_u = \partial\Omega_s \cap \Gamma_u$, and $\Gamma_{st} = \Gamma_s \cap \Gamma_t = \partial\Omega_s \cap \Gamma_t$. That is, Γ_{su} and Γ_{st} are the parts of the boundary Γ_s where the essential and the natural boundary conditions are prescribed respectively. Taking the inner product of Eq. (1) with $\mathbf{v}$ and of Eq. (4a) with $\alpha\mathbf{v}$, integrating the resulting equations over Ω_s and Γ_{su} respectively, adding them, and using the divergence theorem and the natural boundary condition (4b) on Γ_{st}, we obtain

$$\int_{\Omega_s} (\sigma_{ij} v_{i,j} - b_i v_i) d\Omega + \int_{\Gamma_{su}} \alpha (u_i - \overline{u}_i) v_i d\Gamma - \int_{\Gamma_{st}} \overline{t}_i v_i d\Gamma - \int_{\Gamma_{su}} t_i v_i d\Gamma = 0. \tag{5}$$

Here α is a scalar function of $\mathbf{x}$ which is defined on Γ_{su} and can be regarded either as a Lagrange multiplier in which case it is to be determined as a part of the solution of the problem or a preassigned penalty parameter necessary to satisfy the essential boundary conditions on Γ_{su}. In either case, its units are force/(length)^3 so that Eq. (5) is dimensionally correct. Atluri et al. (1999a) have demonstrated that by using a simple nodal degree of freedom transformation on Γ_{su}, the essential boundary conditions can be exactly satisfied without using either Lagrange multipliers or a penalty approach.

In the Galerkin formulation, $\Omega_s = \Omega$ and the test function $\mathbf{v}$ is taken as one of the basis functions defined on Ω which are used to approximate the trial solution $\mathbf{u}$ on Ω. Here the test function $\mathbf{v}$ and the trial solution $\mathbf{u}$ are from different spaces of functions, and hence the formulation is the Petrov-Galerkin. Atluri et al. (1999a) show how, within the context of the MLPG formulation, the subdomains for the trial and the test functions can be of different sizes and shapes; and how the trial and the test functions can be from different or the same spaces, leading to either symmetric or unsymmetric system of equations. In order to obtain two sets of equations for the two components of $\mathbf{u}$, we select two linearly independent functions $\mathbf{v}^{(1)}$ and $\mathbf{v}^{(2)}$ for $\mathbf{v}$ in Eq. (5), and write it in the matrix form as

$$\int_{\Omega_s} \varepsilon_v \sigma d\Omega + \int_{\Gamma_{su}} \alpha \mathbf{v}\mathbf{u} d\Gamma - \int_{\Gamma_{su}} \mathbf{v}\mathbf{t} d\Gamma = \int_{\Gamma_{st}} \mathbf{v}\overline{\mathbf{t}} d\Gamma + \int_{\Gamma_{su}} \alpha \mathbf{v}\overline{\mathbf{u}} d\Gamma + \int_{\Omega_s} \mathbf{v}\mathbf{b} d\Omega. \tag{6}$$

Here ε_v is the matrix of strain components derived from $\mathbf{v}$, and σ is the matrix of stress components derived from the trial solution $\mathbf{u}$. For 2-dimensional problems,

$$\sigma = \begin{Bmatrix} \sigma_{11} \\ \sigma_{22} \\ \sigma_{12} \end{Bmatrix}, \ \varepsilon = \begin{Bmatrix} \varepsilon_{11}^{(1)} & \varepsilon_{22}^{(1)} & 2\varepsilon_{12}^{(1)} \\ \varepsilon_{11}^{(2)} & \varepsilon_{22}^{(2)} & 2\varepsilon_{12}^{(2)} \end{Bmatrix},$$
$$\mathbf{u} = \begin{Bmatrix} u_1 \\ u_2 \end{Bmatrix}, \ \mathbf{v} = \begin{Bmatrix} v_1^{(1)} & v_2^{(1)} \\ v_1^{(2)} & v_2^{(2)} \end{Bmatrix}$$
$$\mathbf{t} = \begin{Bmatrix} t_1 \\ t_2 \end{Bmatrix}, \ \mathbf{b} = \begin{Bmatrix} b_1 \\ b_2 \end{Bmatrix}. \tag{7}$$

Here superscripts (1) and (2) signify, respectively, the quantity derived from test functions $\mathbf{v}^{(1)}$ and $\mathbf{v}^{(2)}$. A simple choice for two linearly independent test functions $\mathbf{v}^{(1)}$ and $\mathbf{v}^{(2)}$ is

$$\mathbf{v} = \begin{Bmatrix} v & 0 \\ 0 & v \end{Bmatrix}. \tag{8}$$

2.3 Trial solutions

Let $\Omega_{\mathbf{x}} \subset \Omega$ be the neighborhood of a point $\mathbf{x} \in \Omega$. We approximate the trial solution $\mathbf{u}^h(\mathbf{x})$ on $\Omega_{\mathbf{x}}$ by

$$u_i^h(\mathbf{x}) = \phi_\alpha(\mathbf{x}) \hat{u}_{\alpha i}, \ (\alpha = 1,2,\ldots,n; \ i = 1,2), \tag{9}$$

where $\phi_1(\mathbf{x})$, $\phi_2(\mathbf{x})$, $\ldots, \phi_n(\mathbf{x})$ are linearly independent functions defined on $\Omega_{\mathbf{x}}$ and $\hat{u}_{\alpha i}$ are $2n$ scalar quantities which are not necessarily associated with the values of $\mathbf{u}^h(\mathbf{x})$ at any point in $\Omega_{\mathbf{x}}$. We use the

Moving Least Squares (MLS) approach to ascertain $\phi_1(\mathbf{x}),\ \phi_2(\mathbf{x}),\ldots,\phi_n(\mathbf{x})$.

Let at every point $\mathbf{x}\in\Omega_{\mathbf{x}}$,

$$u_1^h(\mathbf{x}) = p_\Lambda(\mathbf{x})a_\Lambda(\mathbf{x}),\ (\Lambda = 1,2,\ldots,m), \tag{10}$$

and a similar relation holds for $u_2^h(\mathbf{x})$. Here $\mathbf{p}(\mathbf{x}) = [p_1(\mathbf{x}),\ p_2(\mathbf{x}),\ldots,p_m(\mathbf{x})]$ is a complete monomial basis of order m, $\mathbf{a}(\mathbf{x})$ is an m-dimensional vector valued function of $\mathbf{x}$ whose components are determined by finding an extremal of the following weighted discrete L_2 norm:

$$J(\mathbf{x}) = \sum_{\alpha=1}^{n} w_\alpha(\mathbf{x})[p_\Lambda(\mathbf{x}_\alpha)a_\Lambda(\mathbf{x}) - \hat{u}_{\alpha 1}]^2. \tag{11}$$

Here $w_\alpha(\mathbf{x})$ is the weight function associated with the spatial point $\mathbf{x}_\alpha$, $w_\alpha(\mathbf{x}) > 0$ in its compact support, and $\mathbf{x}_1,\ \mathbf{x}_2,\ldots,\mathbf{x}_n$ are the points in $\Omega_{\mathbf{x}}$ for which $w_\alpha(\mathbf{x}) > 0$. Points $\mathbf{x}_1,\ \mathbf{x}_2,\ldots,\mathbf{x}_n$ are called nodes.

Solving the set of m linear simultaneous equations $\partial J/\partial a_\Lambda(\mathbf{x}) = 0$ for $a_\Lambda(\mathbf{x})$, substituting the solution in Eq. (10) and comparing the result with Eq. (9) we obtain

$$\phi_\alpha(\mathbf{x}) = p_\Gamma(\mathbf{x})[\mathbf{A}^{-1}(\mathbf{x})\mathbf{B}(\mathbf{x})]_{\Gamma\alpha}, \tag{12}$$

$$A_{\Lambda\Gamma}(\mathbf{x}) = \sum_{\alpha=1}^{n} w_\alpha(\mathbf{x})p_\Lambda(x_\alpha)p_\Gamma(x_\alpha), \tag{13}$$

$$B_{\Gamma\alpha}(\mathbf{x}) = p_\Gamma(x_\alpha)w_\alpha(\mathbf{x}),\ \text{no sum on } \alpha. \tag{14}$$

Necessary conditions for the matrix $\mathbf{A}$ to be invertible are that for $\alpha = 1,2,\ldots,m \le n$, $w_\alpha(\mathbf{x}) \neq 0$ for every $\mathbf{x}\in\Omega_{\mathbf{x}}$, and that the n node points $\mathbf{x}_\alpha\in\Omega_{\mathbf{x}}$ used to evaluate $J(\mathbf{x})$ in Eq. (11) are not arranged in a special pattern such as a straight line.

The function $\phi_\alpha(\mathbf{x})$ is called the shape function of the MLS approximation corresponding to the node point $\mathbf{x}_\alpha$. Note that $\phi_\alpha(\mathbf{x}_\beta)$ need not equal $\delta_{\alpha\beta}$ where $\delta_{\alpha\beta}$ is the Kronecker delta. We have assumed the weight function $w_\alpha(\mathbf{x})$ to have the Gaussian distribution, viz.,

$$w_\alpha(\mathbf{x}) = \begin{cases} \dfrac{\exp(-d_\alpha/c_\alpha)^{2k} - \exp(-r_\alpha/c_\alpha)^{2k}}{1-\exp(-r_\alpha/c_\alpha)^{2k}}, & 0 \le d_\alpha \le r_\alpha, \\ 0, & d_\alpha > r_\alpha, \end{cases} \tag{15}$$

there is no sum on the index α, $d_\alpha = |\mathbf{x}-\mathbf{x}_\alpha|$ is the distance from node $\mathbf{x}_\alpha$ to point $\mathbf{x}$, k and c_α are constants, and r_α is the radius of the support of $w_\alpha(\mathbf{x})$. The values of the constants $c_\alpha,\ r_\alpha$, and k may affect the accuracy of computed results and should be chosen carefully. Following Lu et al.'s (1994) recommendation we have taken $k = 1$, c_α equal to the distance to the third nearest neighboring node from the node $\mathbf{x}_\alpha$, and $r_\alpha = 4c_\alpha$; when finding the third nearest neighboring node from the node $\mathbf{x}_\alpha$, nodes equidistant from $\mathbf{x}_\alpha$ are counted once. The support of the weight function, w_α, includes at least m nodes to ensure the invertibility of the matrix $\mathbf{A}$ defined by Eq. (13).

We note that the domain of definition of an MLS approximation for the trial function at a point $\mathbf{x}$, hereafter termed the domain of definition of a point $\mathbf{x}$, is a subdomain which covers all the nodes whose weight functions do not vanish at $\mathbf{x}$. The support of node $\mathbf{x}_\alpha$ is a subdomain, usually taken as a circle of radius r_α, in which the weight function w_α in the MLS approximation, associated with node $\mathbf{x}_\alpha$, is nonzero.

2.4 *Enriched basis functions*

In the application of the meshless method to linear elastic fracture mechanics (LEFM) problems, it is advantageous to add the asymptotic near-tip displacement field to the basis functions so that the stress singularity can be captured without having a very fine nodal mesh around the crack tip. Fleming et al. (1997) first proposed this for the Element Free Galerkin method (EFGM) and called the resulting basis as enriched basis functions. We do this for the MLPG method to study the LEFM problems. In two-dimensional LEFM, both mode-I and mode-II crack-tip fields should be considered. For mode-I deformations, the crack-tip displacements are (Anderson, 1991)

$$\begin{Bmatrix} u_1 \\ u_2 \end{Bmatrix} = \frac{K_I}{2\mu}\sqrt{\frac{r}{2\pi}} \begin{Bmatrix} \cos\dfrac{\theta}{2}\left[\kappa - 1 + 2\sin^2\dfrac{\theta}{2}\right] \\ \sin\dfrac{\theta}{2}\left[\kappa + 1 - 2\cos^2\dfrac{\theta}{2}\right] \end{Bmatrix}, \tag{16a}$$

$$\begin{Bmatrix} \sigma_{11} \\ \sigma_{22} \\ \sigma_{12} \end{Bmatrix} = \frac{K_I}{\sqrt{2\pi r}}\cos\frac{\theta}{2} \begin{Bmatrix} 1 - \sin\dfrac{\theta}{2}\sin\dfrac{3\theta}{2} \\ 1 + \sin\dfrac{\theta}{2}\sin\dfrac{3\theta}{2} \\ \sin\dfrac{\theta}{2}\cos\dfrac{3\theta}{2} \end{Bmatrix}. \tag{16b}$$

For mode-II deformations, the asymptotic displacement fields near the crack-tip are (Anderson, 1991)

$$\left\{ \begin{array}{c} u_1 \\ u_2 \end{array} \right\} = \frac{K_{II}}{2\mu}\sqrt{\frac{r}{2\pi}} \left\{ \begin{array}{c} \sin\frac{\theta}{2}\left[\kappa+1+2\cos^2\frac{\theta}{2}\right] \\ -\cos\frac{\theta}{2}\left[\kappa-1-2\sin^2\frac{\theta}{2}\right] \end{array} \right\}, \tag{17a}$$

$$\left\{ \begin{array}{c} \sigma_{11} \\ \sigma_{22} \\ \sigma_{12} \end{array} \right\} = \frac{K_{II}}{\sqrt{2\pi r}} \left\{ \begin{array}{c} -\sin\frac{\theta}{2}\left(2+\cos\frac{\theta}{2}\cos\frac{3\theta}{2}\right) \\ \sin\frac{\theta}{2}\cos\frac{\theta}{2}\cos\frac{3\theta}{2} \\ \cos\frac{\theta}{2}\left(1-\sin\frac{\theta}{2}\sin\frac{3\theta}{2}\right) \end{array} \right\}. \tag{17b}$$

Here K_I and K_{II} are the stress intensity factors, and depend upon the crack length, the specimen geometry and the applied loading, and (r,θ) are the cylindrical coordinates of a point with the origin located at the crack-tip and the positive angle measured counterclockwise from the axis of the crack. The Kolosov constant κ is related to Poisson's ratio ν by

$$\kappa = \left\{ \begin{array}{ll} 3-4\nu & \text{for plane stress,} \\ \dfrac{3-\nu}{1+\nu} & \text{for plane strain,} \end{array} \right. \tag{18}$$

problems. After using trigonometric identities, one can show that all of the functions in Eqs. (16) and (17) are spanned by the following four basis functions:

$$\sqrt{r}\left\{\cos\frac{\theta}{2},\ \sin\frac{\theta}{2},\ \sin\frac{\theta}{2}\sin\theta,\ \cos\frac{\theta}{2}\sin\theta\right\}. \tag{19}$$

These four basis functions are added to the monomial basis functions in $\mathbf{p}(\mathbf{x})$ to form enriched basis functions. Thus, $\mathbf{p}(\mathbf{x})$ will have either seven or ten basis functions according as it has complete monomials of degree 1 or 2 respectively.

2.5 Visibility and diffraction criteria

The meshless methods usually provide a smooth approximation of a function and its spatial derivatives; however, the displacements are generally discontinuous across a crack. One way to introduce discontinuities in the MLPG approximation is to adopt the visibility criterion proposed by Belytschko et al. (1994). In this approach, a crack is considered to be opaque. When the domain of influence for a weight function is constructed, the line from a point to a node is viewed to be a ray of light. If the ray of light encounters this opaque crack, it is terminated and the point is not included in the domain of influence of the node. For example, consider a crack shown in Fig. 1a. The domain of influence for node P is truncated by this crack, and the shaded area on the opposite side of node P is not included in the domain of influence for node P. This truncation will create a discontinuity in the shape function for node P and thus result in discontinuous displacement fields across the crack. For a node near the crack tip, an additional discontinuity may be produced by the visibility method. For example, the domain of influence for node I is not only cut by the crack line AC, but also truncated by the line AB, which introduces discontinuous shape functions around the crack tip. Even though the shape functions are discontinuous, Krysl and Belytschko (1997) have shown that the method gives convergent solutions.

Another technique to account for discontinuous fields across the crack is the diffraction method proposed by Organ et al. (1996). In this method, the domain of influence for a node near the crack tip is wrapped around its sharp corner. For example, in Fig. 1b, if the line joining a sampling point $\mathbf{x}$ and a node $\mathbf{x}_I$ intersects the crack line and the crack tip is within the domain of influence of the node, then the distance d_α in the expression (15) for the weight function is modified to

$$d_\alpha = \left(\frac{s_1+s_2(\mathbf{x})}{s_0(\mathbf{x})}\right)^{\tilde{\lambda}} s_0(\mathbf{x}) \tag{20}$$

where $s_1 = |\mathbf{x}_I - \mathbf{x}_c|$, $s_2 = |\mathbf{x} - \mathbf{x}_c|$, $s_0 = |\mathbf{x} - \mathbf{x}_I|$, and $\mathbf{x}_c$ is the position vector of the crack tip located at the point C. The parameter $\tilde{\lambda}$ is used to adjust the distance of the support of $w_\alpha(\mathbf{x})$ on the opposite side of the crack. Organ et al. (1996) found that $\tilde{\lambda} = 1$ or 2 performs well in the EFG analysis. Here, we have taken $\tilde{\lambda} = 1$.

2.6 Computation of the stress intensity factors

Rice (1968) found that the component of Eshelby's (1956) energy momentum tensor along the axis of the crack can be used as a fracture parameter when the contour Γ of integration encloses the crack tip. He denoted

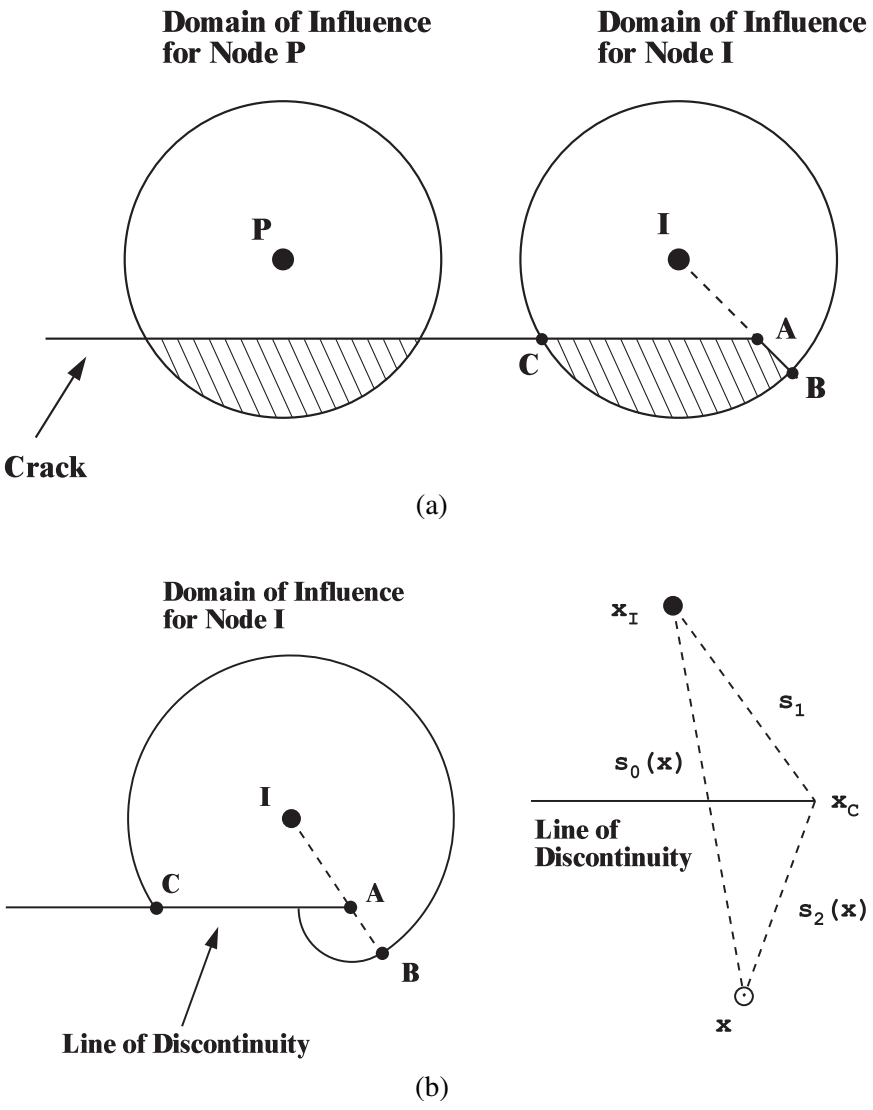

Figure 1 : (a) Domain of influence near a crack tip for the visibility method; (b) Domain of influence near a crack tip for the diffraction method.

this contour integral by J. For the crack along x_1-axis

$$J = \int_\Gamma \left(W\delta_{1j} - \sigma_{ij}\frac{\partial u_i}{\partial x_1} \right) n_j d\Gamma, \tag{21}$$

where $W = \frac{1}{2}\sigma_{ij}\varepsilon_{ij}$ is the strain energy density. For a mixed-mode problem in LEFM, J is related to the stress intensity factors via Irwin's (1957) relation, i.e.,

$$J = \frac{1}{\overline{E}}(K_I^2 + K_{II}^2) \tag{22}$$

where $\overline{E} = E$ for plane stress, $\overline{E} = E/(1-\nu^2)$ for plane strain problems, and E is Young's modulus. Yau et al. (1980) and Shih and Asaro (1988) have used an interaction integral to extract K_I and K_{II} from Eq. (22); the interaction integral is described below.

Consider two equilibrium states of a body with a crack: state 1 the actual state for the given boundary conditions and state 2 an auxiliary state. The interaction integral, $M^{(1,2)}$, for the two equilibrium states is given by

$$M^{(1,2)} = \int_\Gamma \left[W^{(1,2)}\delta_{1j} - \sigma_{ij}^{(1)}\frac{\partial u_i^{(2)}}{\partial x_1} - \sigma_{ij}^{(2)}\frac{\partial u_i^{(1)}}{\partial x_1} \right] n_j d\Gamma, \tag{23}$$

where

$$W^{(1,2)} = \frac{1}{2}(\sigma_{ij}^{(1)}\varepsilon_{ij}^{(2)} + \sigma_{ij}^{(2)}\varepsilon_{ij}^{(1)}), \tag{24}$$

is the mutual strain energy density. For the two superposed equilibrium states, Eq. (21) gives

$$J^{tot} = J^{(1)} + J^{(2)} + M^{(1,2)}. \tag{25}$$

Irwin's relation (22) implies that

$$\begin{aligned} J^{tot} &= \frac{1}{\overline{E}}\left[(K_I^{(1)} + K_I^{(2)})^2 + (K_{II}^{(1)} + K_{II}^{(2)})^2\right], \\ &= J^{(1)} + J^{(2)} + \frac{2}{\overline{E}}(K_I^{(1)}K_I^{(2)} + K_{II}^{(1)}K_{II}^{(2)}). \end{aligned} \tag{26}$$

Equating the right hand sides of Eqs. (25) and (26) we conclude that

$$M^{(1,2)} = \frac{2}{\overline{E}}(K_I^{(1)}K_I^{(2)} + K_{II}^{(1)}K_{II}^{(2)}). \tag{27}$$

The choice (16) for the auxiliary field gives

$$M^{(1,2)} = \frac{2}{\overline{E}}K_I, \tag{28}$$

and the choice (17) for it yields

$$M^{(1,2)} = \frac{2}{\overline{E}}K_{II}. \tag{29}$$

Thus K_I and K_{II} can be computed from the interaction integral by appropriate choices of the auxiliary field. Further details on the use of the M-integrals for crack problems in isotropic media, as well as cracks at anisotropic bimaterial interfaces can be found in Atluri (1997), and Chow et al. (1995).

The line integrals (21) and (23) are often converted into equivalent domain forms for numerical evaluation. Let q be a differentiable function that equals 0 on the closed contour Γ and equals 1 at the crack tip. It can be shown that (e.g. see Nikishkov and Atluri (1987); Moran and Shih (1987); and Anderson (1991))

$$J = \int_A \left(\sigma_{ij}\frac{\partial u_i}{\partial x_1} - W\delta_{1j}\right)\frac{\partial q}{\partial x_j}d\Omega, \tag{30}$$

$$M^{(1,2)} = \int_A \left(\sigma_{ij}^{(1)}\frac{\partial u_i^{(2)}}{\partial x_1} + \sigma_{ij}^{(2)}\frac{\partial u_i^{(1)}}{\partial x_1} - W^{(1,2)}\delta_{1j}\right)\frac{\partial q}{\partial x_j}d\Omega, \tag{31}$$

where A is the area enclosed by the contour Γ. This approach of evaluating K_I and K_{II} is called the equivalent domain integral (EDI) method, is often used in the finite element work, and has been employed by Lu et al. (1994) in the EFG method. It requires the discretization of the domain A into either ficticious cells or finite elements. However, the determination of K_I and K_{II} from Eqs. (23), (28) and (29) keeps the method purely meshless. Kim and Atluri (2000) use the EDI method in the context of the meshless MLPG formulation.

3 Computation and Discussion of Results

We have developed a computer code based on the aforestated equations. The code has been validated by comparing computed results with the analytical solution for the following three problems: a cantilever beam loaded by tangential tractions at the unclamped edge, an infinite plate with a circular hole subjected to uniformly distributed tensile tractions at infinity, and a circular hollow cylinder subjected to a pressure loading on the inner surface. In each case the computed solution was found to essentially coincide with the analytical solution of the problem. For the cantilever beam problem, as also pointed out by Atluri and Zhu (2000), the MLPG method gave exact results even for Poisson's ratio = 0.4999; the FE method exhibits locking phenomenon for this case and significantly underestimates the tip deflection of the cantilever beam. Here we describe results for five other problems. In each case, there is no body force, and the penalty function α defined on Γ_{su} in Eq. (5) is taken to be a constant, and is set equal to $10^5 E/\ell$ where ℓ is a typical length in the problem. The test function $v(\mathbf{x})$ (cf. Eq. (8)) is set equal to the weight function $w_\alpha(\mathbf{x})$ of the MLS approximation, with the radius r_0 of the local domain Ω_s taken equal to the radius r_α of the support of the weight function. If the union of all local domains covers the global domain, i.e., $\cup\Omega_s \supset \Omega$, the equilibrium equations and the boundary conditions are satisfied respectively in Ω and on Γ. This is ensured by selecting an Ω_s for each node $\mathbf{x}_\alpha \in \Omega$ and taking r_0 large enough. While evaluating integrals on Ω_s and Γ_s, 8×8 and 8 Gauss points are employed respectively. The two linear algebraic equations resulting from Eq. (6) are assembled, and solved for $\hat{u}_i$. Displacements and hence strains and stresses at any point $\mathbf{x} \in \Omega$ can then be computed from Eqs. (9), (3) and (2) respectively. We use (i) the quadratic (with and without the enriched) basis functions, (ii) either the visibility or the diffraction criterion, and (iii) Eq. (27) with the near crack tip solution as the auxiliary field to com-

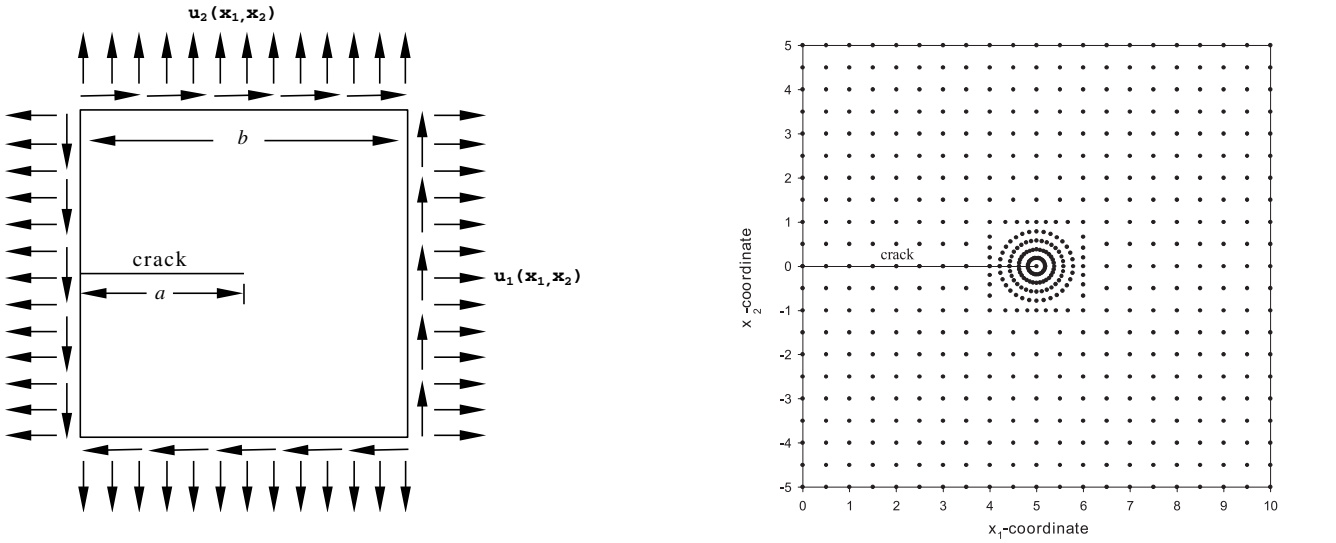

(a) (b)

Figure 2 : (a) An edge-cracked square plate subjected to mode-I displacement field at its edges; (b) The nodal mesh with 590 nodes.

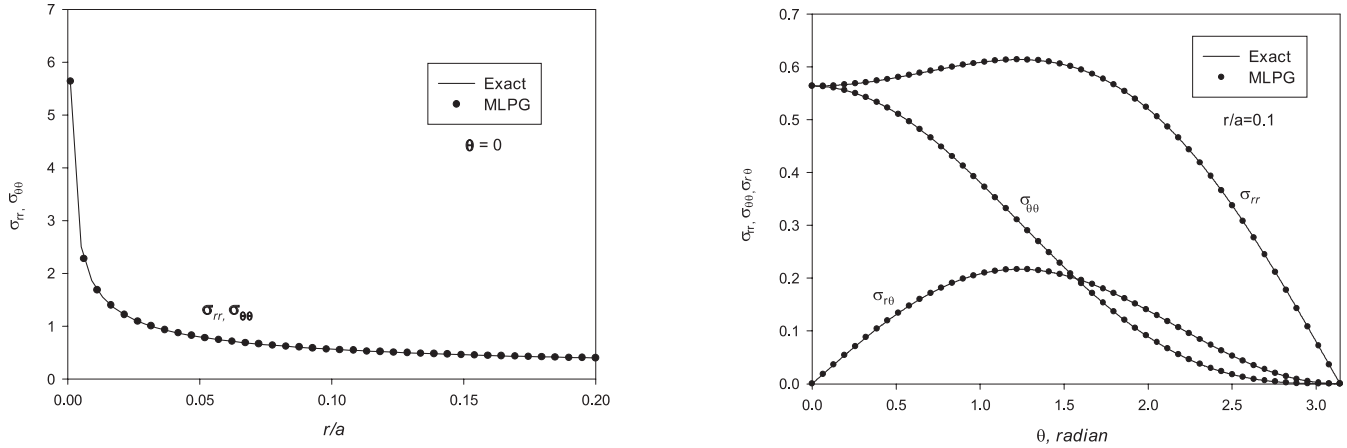

(a) (b)

Figure 3 : (a)Axial variations of σ_{rr} and $\sigma_{\theta\theta}$ ahead of the crack tip; (b) Angular variation of stresses at $r/a = 0.1$.

pute the stress intensity factors.

3.1 Near-tip mode-I stress fields

We analyze plane strain deformations of a single edge-cracked square plate of side b and crack length a with $b = 2a = 10$ units, $E = 1000$ units and $\nu = 0.3$. Both tangential and normal displacements given by Eqn. (16a) and $K_I = 1$ are prescribed on the four bounding edges. Figure 2a shows a sketch of the problem studied and Fig. 2b displays the layout of the 590 nodes; the nodal mesh is fine near the crack tip. Rao and Raman (2000) have scrutinized this problem by the EFG method in conjunction with the enriched basis functions and the diffraction criterion, and employed uniformly spaced mesh of 175

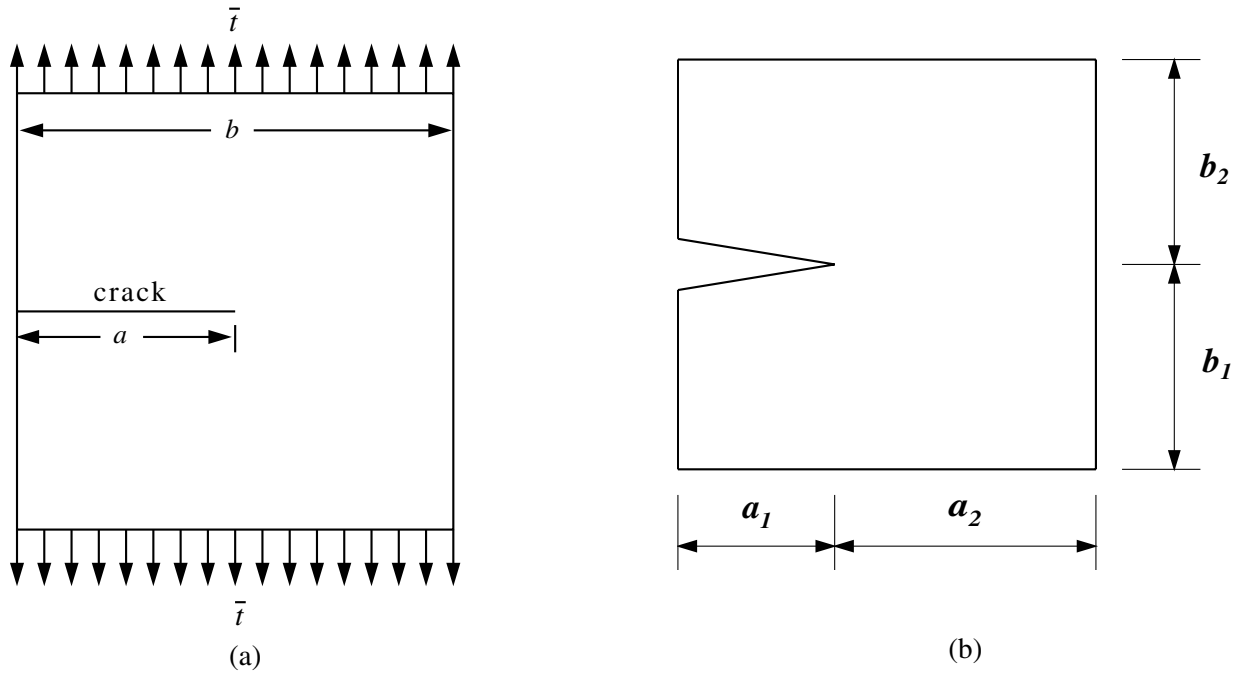

Figure 4 : (a) An edge-cracked square plate loaded by uniformly distributed tensile surface tractions on edges parallel to the crack; (b) The contour of integration for the evaluation of the J-integral and the interaction integral.

nodes with 13 nodes on each side. They used weight functions based on the Student's t-distribution. For the weight functions, the values of d_α, c_α, r_α, k and $\tilde{\lambda}$ used herein and the enriched basis functions, stresses near the crack-tip computed with the uniformly spaced mesh of 175 nodes deviated somewhat from the exact solution of the problem. However, with the nodal mesh of Fig. 2b and as shown in Fig. 3a, the variations of σ_{rr} and $\sigma_{\theta\theta}$ with the distance from the crack tip of points on the crack axis match very well with the analytical solution (16b) of the problem. Also, for $r/a = 0.1$, the variation with the angle, θ, of the computed values of σ_{rr}, $\sigma_{\theta\theta}$ and $\sigma_{r\theta}$ agree very well with those obtained from the analytical solution (16b). Here σ_{rr}, $\sigma_{\theta\theta}$ and $\sigma_{r\theta}$ are the radial, the circumferential (or the hoop) and the shear stresses respectively. Similar accuracy of the stresses was also demonstrated by Fleming et al. (1997) and Rao and Raman (2000) with the EFG method.

3.2 Edge-cracked plate loaded in tension

Plane strain deformations of an edge-cracked square plate, shown in Fig. 4a with $b = 10$, $a = 5$, $E = 1000$, $\nu = 0.25$ and $\bar{t} = 1$ are analyzed. Due to the symmetry of the problem about the horizontal centroidal axis, deformations of only the upper half of the plate with the nodal mesh of Fig. 2b are studied.

The expression for K_I given in Gdoutos (1993) is

$$K_I = \bar{t}\sqrt{\pi a}\left[1.12 - 0.23\frac{a}{b} + 10.55\left(\frac{a}{b}\right)^2 - 21.72\left(\frac{a}{b}\right)^3 + 30.39\left(\frac{a}{b}\right)^4\right] \tag{32}$$

Thus, for the plate problem being studied, $K_I = 11.2$. We have listed in Table 1 computed values of the stress intensity factor K_I for different contours Γ and without using the enriched basis functions; the contour is shown in Fig. 4b. It is clear that the computed value of K_I is essentially independent of the contour, and it differs from the analytical value by less than 2.8%. The value of K_I computed with the contour integral is slightly closer to the analytical value than that obtained by the EDI method. In the evaluation of the domain integrals (30) and (31), we took

$$q(x_1,x_2) = (x_1 - a_2)(x_1 + a_1)(x_2 - b_2)(x_2 + b_1)/(a_1 a_2 b_1 b_2),$$

with the origin of the $x_1 - x_2$ coordinate axes at the crack tip; a_1, a_2, b_1 and b_2 are defined in Fig. 4b.

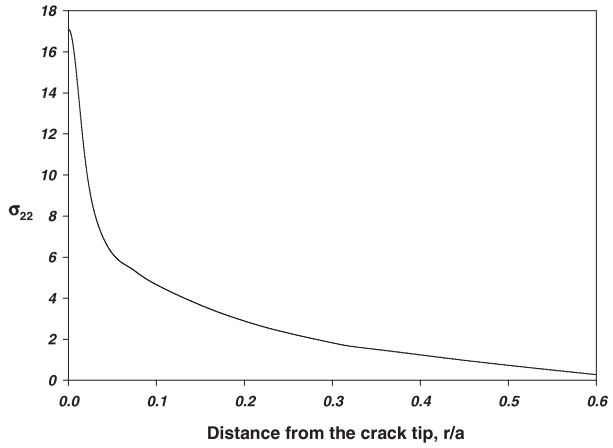

(a)

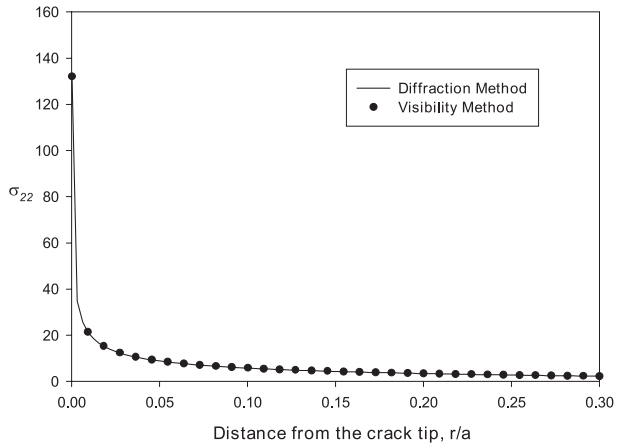

(b)

Figure 5 : (a) Variation of σ_{22} at points on the axis of the crack with their distance from the crack tip computed without using enriched basis functions; (b) Variation of σ_{22} at points on the axis of the crack with their distance from the crack tip computed with the enriched basis funcitons.

Although an accurate value of the stress intensity factor has been determined by using a fine nodal mesh near the crack tip and without using the enriched basis functions, the singular stress fields may not be accurately computed. As shown in Fig. 5a, the normal stress σ_{22} near the crack tip is finite and does not exhibit the $1/\sqrt{r}$ singularity. Therefore, we use the enriched basis functions, and model the entire edge-cracked plate because we adopt either the visibility or the diffraction criterion. Figure 5b evinces the variation of the normal stress σ_{22} along the horizontal line passing through the crack tip. The stress reaches very large values near the crack tip, and both the visibility and the diffraction criteria give virtually identical results. As was found by Belytschko et al. (1996) for the EFG method, the solution computed with the visibility criterion in the MLPG formulation converges. Figure 6 exhibits the angular variation of the radial and the hoop stresses at points located at a radial distance of 0.5 $(r/a = 0.1)$ from the crack tip. We note that the stress distributions obtained with the visibility and the diffraction criteria are identical.

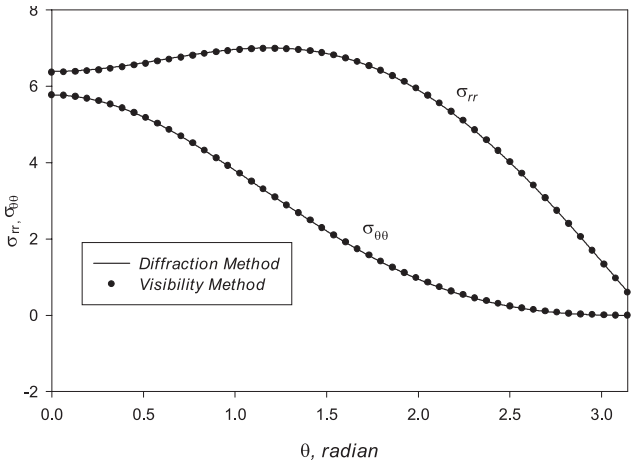

Figure 6 : Angluar variation of the radial stress, σ_{rr}, and the hoop stress, $\sigma_{\theta\theta}$, around the crack tip obtained by using the visibility and the diffraction methods; here $r/a = 0.1$.

3.3 Double edge-cracked plate loaded in tension

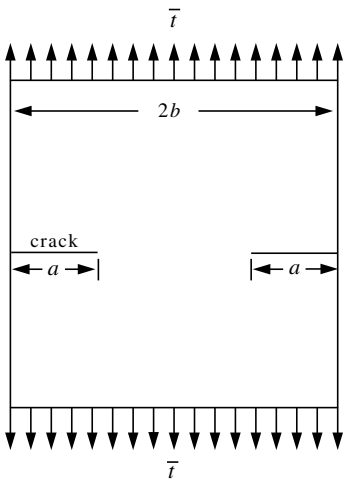

(a)

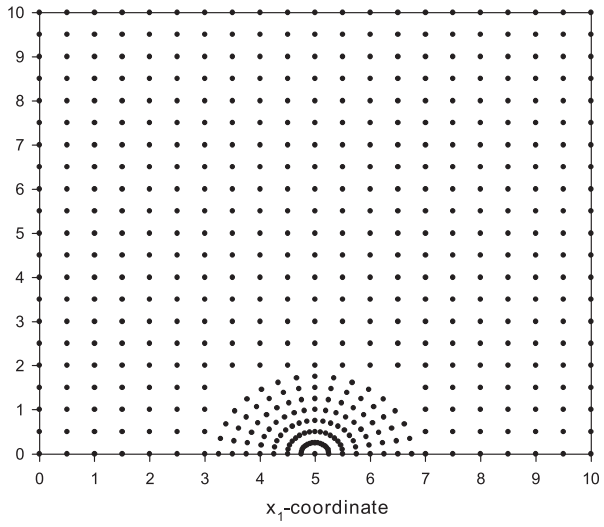

(b)

Figure 7 : (a) A double edge-cracked square plate with edges parallel to the crack loaded by uniformly distributed tensile surface tractions; (b) The nodal mesh with 533 nodes for one-half of the double edge-cracked plate.

We now study deformations of a square plate with cracks emanating from the vertical edges and subjected to the uniform tensile tractions ($\bar{t} = 1$) at the upper and the lower horizontal surfaces; a schematic sketch of the problem studied is shown in Fig. 7a. We only give results for the stress intensity factor since the stress fields around the crack tip are similar to those of the example 3.2.

Due to the symmetry of the problem about the horizontal and the vertical centroidal axes, we consider a quarter of the plate. The nodal mesh used to analyze the problem is shown in Fig. 7b. We presume that a plane strain state of deformation prevails in the plate and set $E = 1000$, $\nu = 0.3$, $b = 10$ and $a = 5$. From the solution given in Gdoutos (1993) we obtain

$$K_I = \bar{t}\sqrt{\pi a}\left[1.12 + 0.2\frac{a}{b} - 1.2\left(\frac{a}{b}\right)^2 + 1.93\left(\frac{a}{b}\right)^3\right] = 4.65.$$

Values of K_I computed with the MLPG method without employing the quadratic polynomial enriched basis functions and by using different contours (a_1, a_2, b_1 and b_2 are defined in Fig. 4b) are summarized in Table 2. For the first seven contours considered, the value of K_I computed by the EDI method differs from its analytical value by less than 3.2%. The value of K_I computed with the contour integrals has an error of about 6%. For the contour of integration close to the crack tip, the EDI method has a larger error than the contour integral method. The value of K_I computed from the y-intercept of the plot of $ln\sigma_{22}(r,0)$ vs. $ln\, r$ with the solution obtained using the enriched basis functions was found to be 4.66 which differs from the analytical value by 0.2%.

3.4 Edge-cracked plate under mixed-mode loading

A schematic sketch of the problem studied is exhibited in Fig. 8a, and the nonuniform mesh of 621 nodes used to analyze the problem is shown in Fig. 8b. The bottom edge of the plate is rigidly clamped while the top edge is subjected to uniformly distributed tangential tractions, $\bar{t} = 1$. We set $w = 7$ units, $h = 14$ units, and the crack length $a = 3.5$ units. A plane strain state of deformation is assumed to prevail in the plate. The stress intensity factors K_I and K_{II} computed by using Eqns. (28) and (29) respectively, and the fully enriched quadratic basis functions in a region of radius 2, transition basis functions within an annular region of inner and outer radii of 2 and 4 respectively, and regular basis functions elsewhere are listed in Table 3; lengths a_1, a_2, b_1 and b_2 are illustrated in Fig. 4b. The reference values, $K_I = 34.0$ units and $K_{II} = 4.55$ units, taken from Wilson (1969), compare very well with those computed from Eqns. (28) and (29)

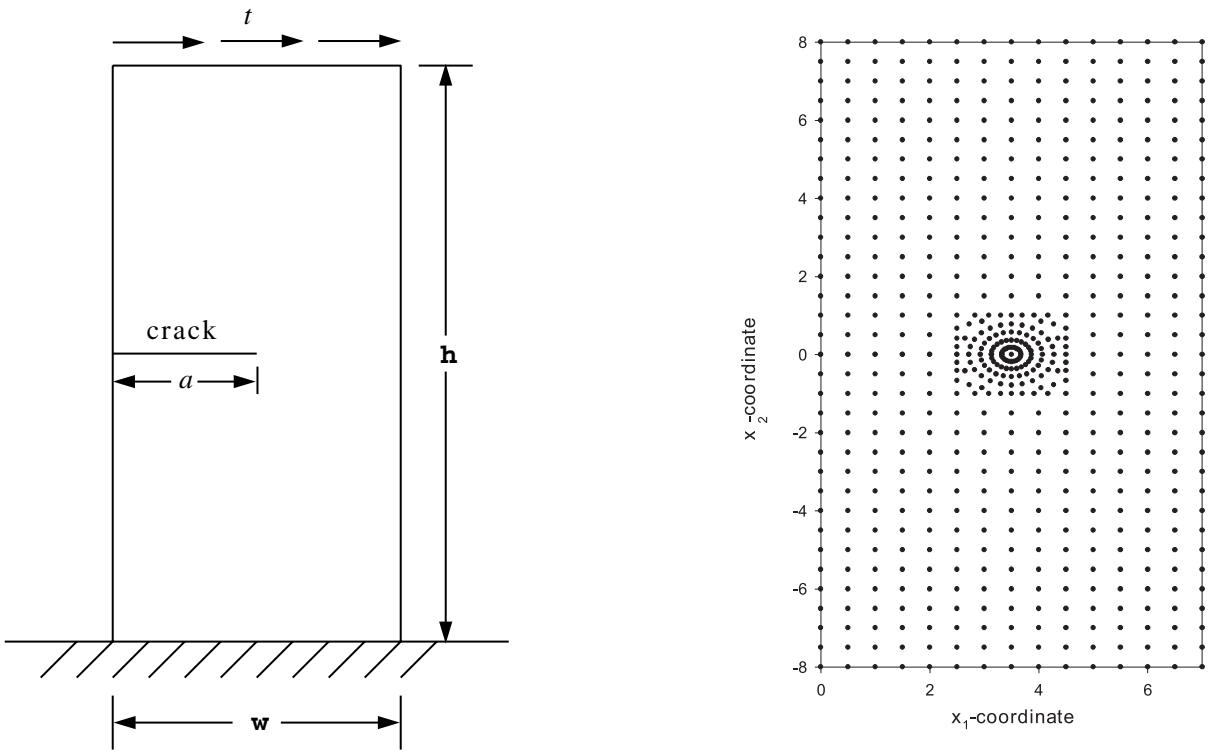

Figure 8 : (a) An edge-cracked plate under mixed-mode loading; (b) The nodal mesh of 621 nodes.

with either the EDI method or the contour integrals. The results are virtually independent of the domain size and the difference between the computed and the reference values of K_I and K_{II} is less than 1.25%. Similar results have been obtained by Rao and Raman (2000) and Fleming et al. (1997) with the EFG method.

3.5 Double edge-notched plate with the edge between the notches loaded in compression

Kalthoff and Winkler (1987) studied transient deformations of a double edge-notched plate with the edge between the notches loaded by a fast moving cylindrical projectile. Here we analyze its quasistatic deformations. A schematic sketch of the problem is depicted in Fig. 9a. We assume that a plane strain state of deformation prevails in the plate, and take $E = 210$ GPa, $\nu = 0.29$, the notch tip radius = 0.15 mm, the applied normal traction $\overline{t} = 200$ MPa, and tangential tractions on this surface = 0. The remaining bounding surfaces of the plate and of the notch are traction free. Deformations of only the upper half of the plate are analyzed with the symmetry boundary conditions imposed on the horizontal centerline of the plate and the rightmost point on this line rigidly clamped. Figure 9b exhibits the nonuniform nodal mesh of 3632 nodes with 25 nodes on the surface of the circular notch tip (cf. Fig. 9c). The visibility method is adopted to account for the discontinuous fields across the notch. Since the nature of the singular fields near the notch tip is unknown, enriched basis functions are not used.

The MLPG results are compared with the finite element (FE) solution computed with four node quadrilateral elements with the same nodes used in the two analyses. Figure 10a depicts the variation of σ_{22} and σ_{12} at points on the axis of the notch and lying ahead of the notch tip; the MLPG and the FE results virtually coincide. The maximum value of $|\sigma_{12}|$ occurs at a point slightly ahead of the notch tip. Note that the axial variation of σ_{12} exhibits a boundary layer like phenomenon near the notch tip. Figure 10b evinces the angular variation of the maximum principal tensile stress and the maximum shear stress at

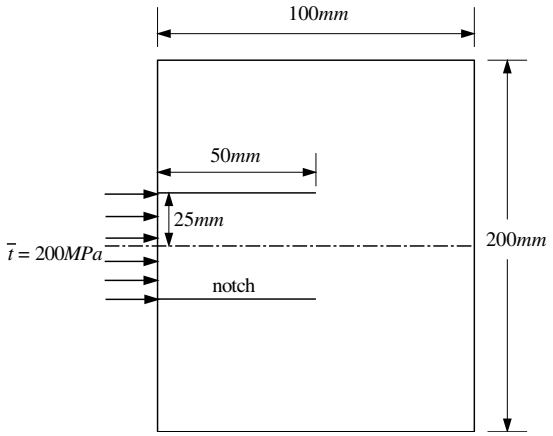

(a)

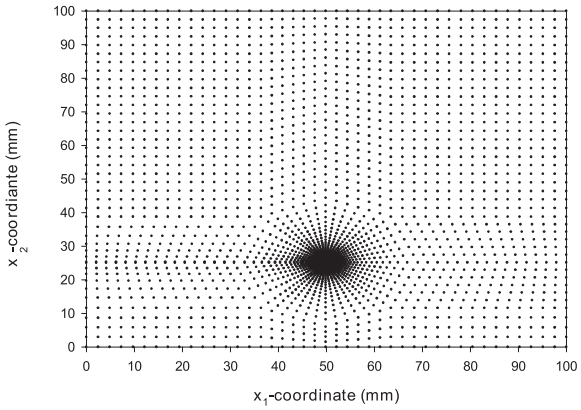

(b)

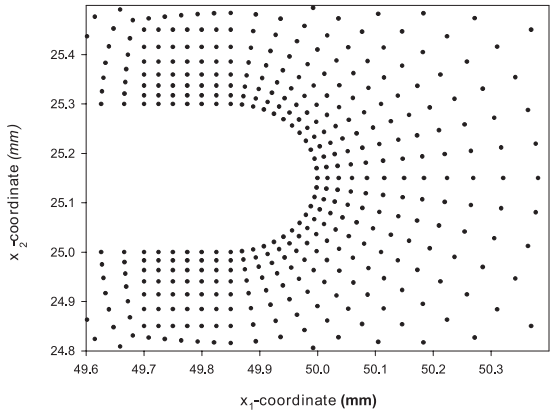

(c)

Figure 9 : (a) A schematic sketch of the double edge-notched plate problem; (b) The nodal mesh for the upper half of the double edge-notched plate; (c) The nodal mesh around the circular notch tip of radius 0.15 mm.

points on the surface of the notch tip. It is clear that the MLPG and the FE solutions agree qualitatively but their magnitudes differ slightly; however, the two solutions predict the same angular locations (70° and -57° respectively) of the points where the maximum principal tensile stress and the maximum shear stress occur; these angular locations are virtually the same as those found by Batra and Gummalla (2000) in the transient analysis of the thermoviscoplastic problem. Once limiting values of these stresses are reached, a brittle failure will ensue from the point where the maximum principal tensile stress occurs and a ductile failure from the location of the maximum shear stress. The maximum principal tensile stress and the maximum shear stress at points on the surface of the notch tip equal approximately ten times the magnitude of the applied uniform normal traction.

We have plotted in Fig. 11, on the logarithmic scale, the variations, at points on the axis of the notch, of $|\sigma_{22}|$ and $|\sigma_{12}|$ with the distance, r, from the notch tip. The slopes of both curves equal $(-1/2)$ signifying the $1/\sqrt{r}$ singularity of the stress fields near the notch tip. Thus the deformation fields close to the tip of the circular notch of radius 0.15 mm seem to behave as if the notch were a sharp crack. Values of the stress intensity factors computed from the y-intercepts of these curves and normalized by the applied normal traction of 200 MPa are $\overline{K}_I = -2.24\sqrt{mm}$ and $\overline{K}_{II} = -4.39\sqrt{mm}$. The mode-mixity parameter, $m^e = \frac{2}{\pi}\tan^{-1}\left(\frac{K_I}{K_{II}}\right)$, at the notch tip equals 0.3 which is close to the analytical value of 0.25 found by Lee and Freund (1990) for the dynamic problem who took Poisson's ratio, $\nu = 0.25$. Lee and Freund showed that the mode mixity parameter stayed unchanged till a wave reflected from the right free edge arrived at the notch tip. Thus the deformations near the notch tip are K_{II} dominated. The three-dimensional analysis of the transient thermoviscoplastic problem by Batra and Ravisankar (2000) showed that there is a noticeable K_{III} deformation field adjacent to the front and the back faces of the plate. The plane strain state of deformation prevails in the middle 75% of the thickness of the plate. In Fig. 10b we have also exhibited the stresses computed by taking $K_I = \overline{K}_I\bar{t}$ and $K_{II} = \overline{K}_{II}\bar{t}$ in Eqns. (16b) and (17b) respectively, and adding like components from the two stress fields. It is clear that the stress fields so obtained do not agree even qualitatively with those computed by the MLPG and the FE methods. It suggests

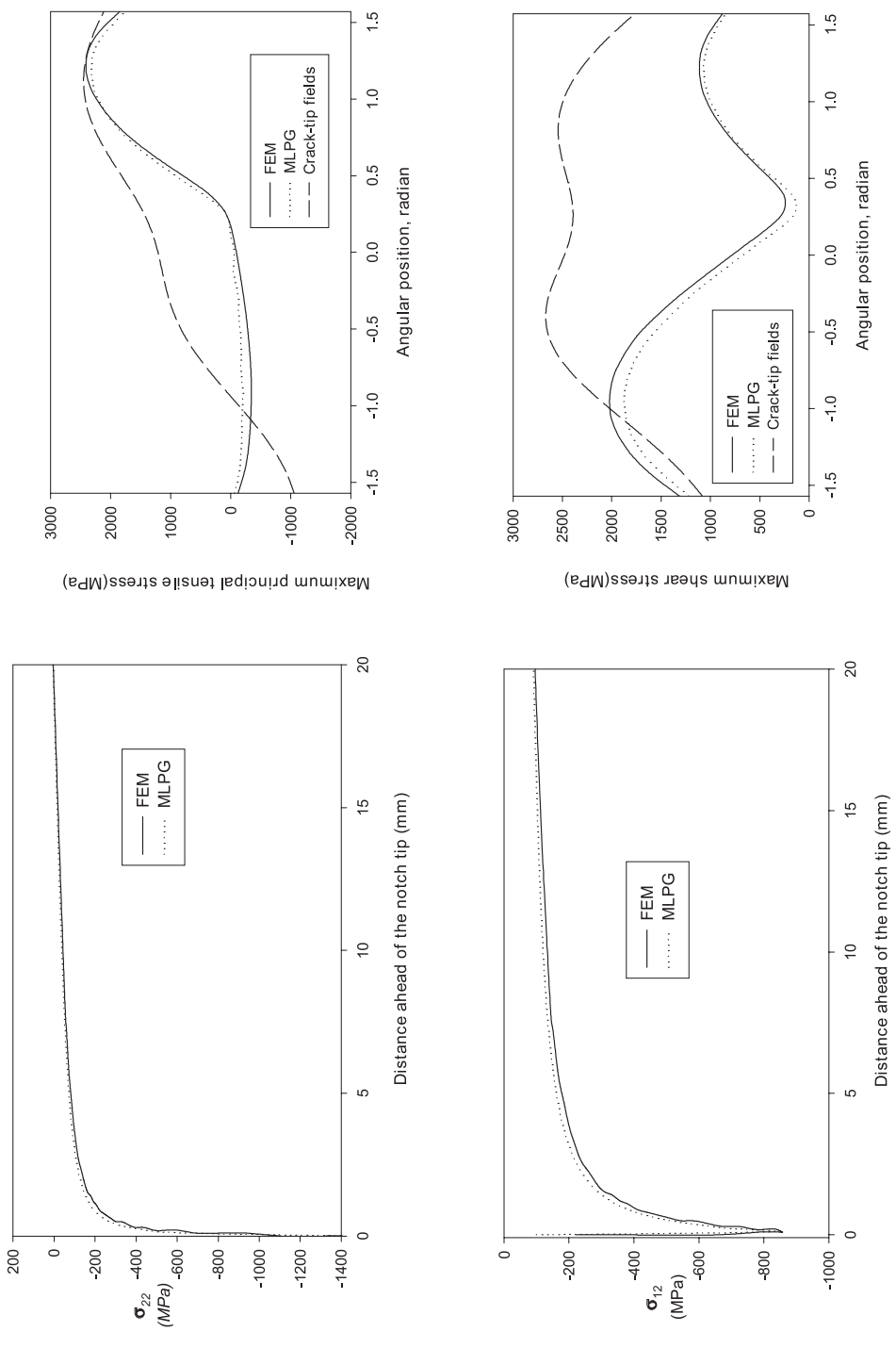

Figure 10 : (a) Variation at points on the axis of the notch tip of (i)σ_{22} and (ii)σ_{12} with the distance from the notch tip; (b) Angular variation at points on the surface of the circular notch tip of the maximum principal tensile stres and the maximum shear stress.

that the stress fields near a notch tip can not be derived from those near a crack tip. However, the stress intensity factors K_I and K_{II} determined from Eqns. (28) and (29) with $M^{(1,2)}$ evaluated from Eqn. (23) are found to be essentially independent of the contour Γ of integration, and their values equal -461 and $-904 N/mm^{3/2}$ respectively. These values are close to those found by the stress extrapolation method, i.e., y-intercepts of straight lines in Fig. 11. The energy release rate computed from Eqn. (21) equals 4490 N/mm. Whereas in Kalthoff's experimental set up and in the numerical simulations of the transient problem, the plate is free to move in the direction of impact, in the static problem studied herein the rigid motions are ruled out. Besides neglecting the effect of inertia forces in the static problem, boundary conditions are not identical in the static and the dynamic problems.

4 Conclusions

We have enriched the polynomial basis functions with the crack tip singular fields and incorporated the visibility and the diffraction criteria, respectively, of Belytschko et al. (1994) and Organ et al. (1996) into the MLPG approach of Atluri and Zhu (1998, 2000) to successfully compute singular fields by the MLPG method.The stress intensity factors computed by using either the contour integrals or the equivalent domain integral method in a single and a double edge-cracked square plate loaded by uniformly distributed either tangential or normal surface tractions on the edges parallel to the crack match well with their reference values. The singular stress fields near the crack tip computed with the MLPG method and the enriched basis functions exhibit the $\sqrt{r}$ singularity, and agree well with those found from the analytical solution. The angular variations of the stress fields computed with the visibility and the diffraction criteria are found to be virtually indistinguishable from each other. For a double edge-notched plate with the edge between the two notches loaded by a uniformly distributed normal traction, the stress fields near the circular notch tip of radius 0.15 mm exhibit the $1/\sqrt{r}$ singularity. Here r is the distance from the notch tip of a point located on the axis of the notch. The mode I and mode II stress intensity factors normalized by the magnitude of the applied normal surface traction equal -2.24 and $-4.39\sqrt{mm}$ respectively.

Acknowledgement: This work was supported in part by the ONR grant N00014-98-1-0300 to Virginia Polytechnic Institute and State University with Dr. Y. D. S. Rajapakse as the program manager.

References

Anderson, T. L. (1991): Fracture Mechanics: *Fundamental and Applications* (1st Ed.) CRC Press.

Atluri, S. N. (1997): *Structural Integrity and Durability*. Tech. Science Press, Forsyth, GA.

Atluri, S. N.; Zhu, T. (1998): A new Meshless Local Petrov-Galerkin (MLPG) approach in computational mechanics. *Computational Mechanics*, vol. 22, pp. 117-127.

Atluri, S. N.; Kim, H. G.; Cho, J. Y. (1999a): A critical assessment of the truly meshless local Petrov-Galerkin (MLPG) and local boundary integral equation (LBIE) methods. *Computational Mechanics*, vol 24, pp. 348-372.

Atluri, S. N.; Cho, J. Y.; Kim, H. G. (1999b): Analysis of thin beams, using the meshless local Petrov-Galerkin method, with generalized moving least squares interpolants. *Computational Mechanics*, vol. 24, pp. 334-347.

Atluri, S. N.; Zhu, T. (2000): The Meshless Local Petrov-Galerkin (MLPG) approach for solving problems in elasto-statics. *Computational Mechanics*, vol. 25, pp. 169-179.

Batra, R. C.; Gummalla, R. R. (2000): Effect of material and geometric parameters on deformations near the notch tip of a dynamically loaded prenotched plate. *International Journal of Fracture*, vol. 101, pp. 99-140.

Batra, R. C.; Ravisankar, M. V. S. (2000): Three dimensional numerical simulation of the Kalthoff problem. *International Journal of Fracture*, vol. 105, pp. 161-186.

Belytschko, T.; Lu, Y. Y.; Gu, L. (1994): Element-free Galerkin methods. *International Journal for Numerical Methods in Engineering*, vol. 37, pp. 229-256.

Belytschko, T.; Krongauz, Y.; Fleming, M.; Organ, D. J.; Liu, W.K. (1996): Smoothing and accelerated computations in the element free Galerkin method. *Journal of Computational and Applied Mathematics*, vol. 74, pp. 111-126.

Belytschko, T.; Krongauz, Y.; Organ, D.; Fleming, M.; Krysl, P. (1996): Meshless methods: An overview

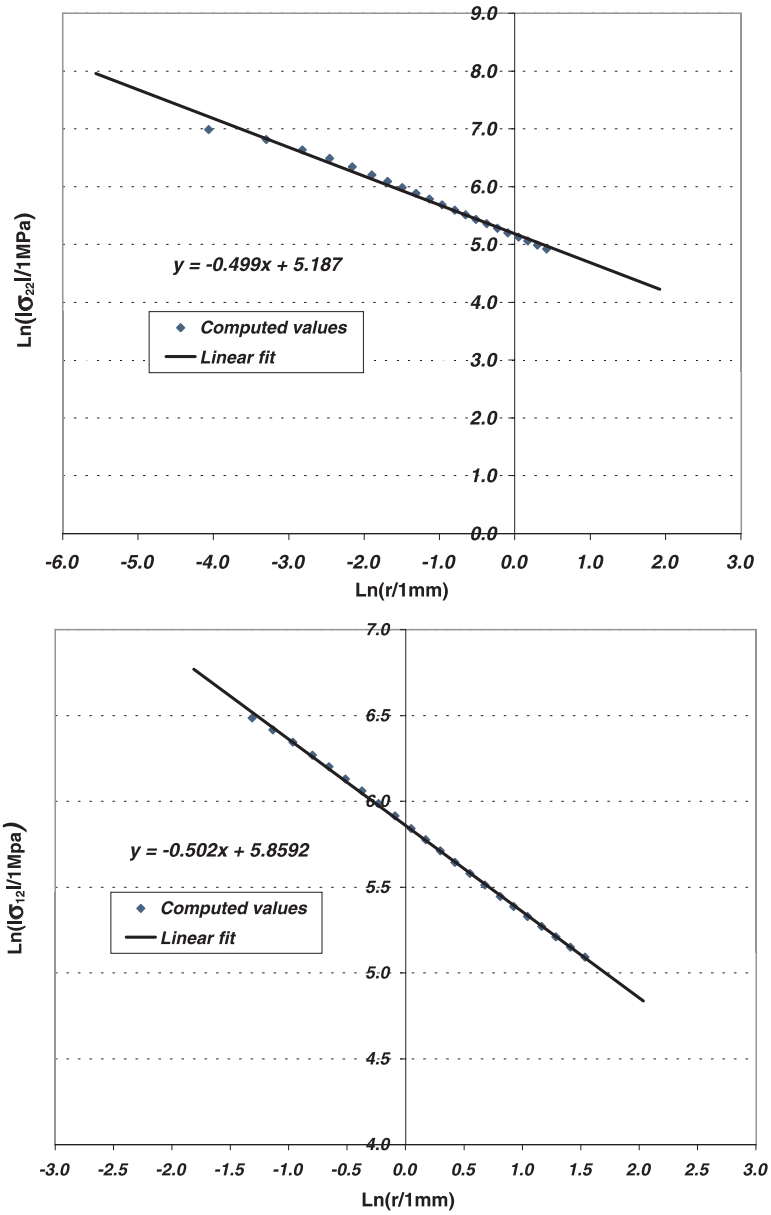

Figure 11 : A logarithmic plot of the variations at points on the axis of the notch tip of (a)σ_{22} and (b)σ_{12} with the distance from the notch tip.

Table 1 : Comparison of analytical values of the stress intensity factor for a single edge-cracked plate loaded in tension with those computed by using the contour and the equivalent domain integrals.

Domain				$K_I^{\text{numerical}}/K_I^{\text{analytical}}$	
a_1	a_2	b_1	b_2	**EDI method**	**Contour**
3	3	3	3	0.9768	0.9804
2	2	2	2	0.9723	0.9821
2.5	2.5	2.5	2.5	0.9750	0.9795
2	2	3	3	0.9786	0.9830
2.5	2.5	3.6	3.6	0.9795	0.9821
1.5	1.5	2.2	2.2	0.9741	0.9848
3	3	4.5	4.5	0.9804	0.9821

Table 2 : Comparison of analytical values of the stress intensity factor for a double edge-cracked plate loaded in tension with those computed by using the contour and the equivalent domain integrals.

Domain				$K_I^{\text{numerical}}/K_I^{\text{analytical}}$	
a_1	a_2	b_1	b_2	**EDI method**	**Contour**
3	3	3	3	1.0194	1.0495
2	2	2	2	1.0108	1.0538
2.5	2.5	2.5	2.5	1.0172	1.0516
2	2	3	3	1.0280	1.0624
2.5	2.5	3.6	3.6	1.0323	1.0624
1.5	1.5	1.5	1.5	1.0001	1.0495
1.5	1.5	2.2	2.2	1.0194	1.0624
0.75	0.75	0.75	0.75	0.9591	1.0473

Table 3 : Comparison of reference values of stress intensity factors for a single edge-cracked plate loaded by tangential tractions with those computed by using the contour and the equivalent domain integrals.

Domain				$K_I^{\text{numerical}}/K_I^{\text{analytical}}$		$K_{II}^{\text{numerical}}/K_{II}^{\text{analytical}}$	
a_1	a_2	b_1	b_2	**EDI method**	**Contour**	**EDI method**	**Contour**
1	1	1	1	1.0089	1.0074	0.9978	0.9980
1.4	1.4	2	2	1.0068	1.0055	0.9974	0.9945
2	2	2	2	1.0065	1.0051	0.9969	0.9954
2.8	2.8	3	3	1.0064	1.0064	0.9965	0.9960
3	3	3	3	1.0064	1.0057	0.9965	0.9974
3.5	3.5	3.5	3.5	1.0065	1.0090	0.9963	0.9903
3.5	3.5	5	5	1.0067	1.0103	0.9960	0.9908
3.5	3.5	6.5	6.5	1.0067	1.0105	0.9960	0.9877

and recent developments. *Computer Methods in Applied Mechanics and Engineering*, vol. 139, pp. 3-47.

Chow, W.-T.; Beom, H. G.; Atluri, S. N. (1995): Calculation of stress intensity factors for an interfacial crack between dissimilar anisotropic media using a hybrid element method and the mutual integral. *Computational Mechanics*, vol. 15, pp. 546-557.

Eshelby, J. D. (1956): The continuum theory of lattice defects. *Solid State Physics*, vol. 3, pp. 79-141.

Fleming, M.; Chu, Y.; Moran, B.; Belytschko, T. (1997): Enriched element-free Galerkin methods for crack tip fields. *International Journal for Numerical Methods in Engineering*, vol. 40, pp. 1483-1504.

Gdoutos, E. E. (1993): Fracture Mechanics: an Introduction. Kluwer Academic Publishers.

Irwin, G. R. (1957): Analysis of stresses and strains near the end of a crack traversing a plate. *Journal of Applied Mechanics*, vol. 24, pp. 361-364.

Kalthoff, J. F.; Winkler, S. (1987): Failure mode transition at high strain rate of shear loading. In Chiem CY, Kunze HD, Meyer LW, editors, *International Conference on Impact Loading and Dynamic Behavior of Materials, Vol. 1*, pp. 185-195.

Kim, H. G.; Atluri, S. N. (2000): Arbitrary placement of secondary nodes, and error control in the meshless local Petrov-Galerkin (MLPG) method. *Computer Modeling in Engineering and Sciences*, vol. 1, pp. 11-32.

Krysl, P.; Belytschko, T. (1997): Element-free Galerkin: Convergence of the continuous and discontinuous shape functions. *Computer Methods in Applied Mechanics and Engineering*, vol. 148, pp. 257-277.

Lin, H; Atluri, S. N. (2000): Meshless local Petrov-Galerkin (MLPG) method for convection-diffusion problems. *Computer Modeling in Engineering and Sciences*, vol. 1, pp. 45-60.

Lu, Y. Y.; Belytschko, T.; Gu, L. (1994): A new implementation of the element free Galerkin method. *Computer Methods in Applied Mechanics and Engineering*, vol. 113, pp. 397-414.

Moran, B; Shih, C. F. (1987): Crack tip and associated domain integrals from momentum and energy balance. *Engineering Fracture Mechanics*, vol. 27(6), pp. 615-641.

Nikishkov, G. P.; Atluri, S. N. (1987): Calculation of fracture mechanics parameters for an arbitrary 3-D crack by the equivalent domain integral method. *Int. J. Num. Method. Engg.*, vol. 24, pp. 1801-1822.

Organ, D. J.; Fleming, M.; Belytschko, T. (1996): Continuous meshless approximations for nonconvex bodies by diffraction and transparency. *Computational Mechanics*, vol. 18, pp. 225-235.

Rao, B. N.; Rahman, S. (2000): An efficient meshless method for fracture analysis of cracks. *Computational Mechanics*, vol. 26, pp. 298-308.

Rice, J. R. (1968): A path independent integral and the approximate analysis of strain concentration by notches and cracks. *Journal of Applied Mechanics*, vol. 35, pp. 379-386.

Shih, C. F.; Asaro, R. J. (1988): Elastic-plastic analysis of cracks on bimaterial interfaces: Part I - small scale yielding. *Journal of Applied Mechanics*, vol. 55, pp. 299-316.

Yau, J. F.; Wang, S. S; Corten, H. T. (1980): A mixed-mode crack analysis of isotropic solids using conservation laws of elasticity. *Journal of Applied Mechanics*, vol. 47, pp. 335-341.